Proceedings World Geothermal Congress 2015
Melbourne, Australia, 19-25 April 2015

Effects of Carbon Dioxide Dissolved in Geothermal Water on Reservoir Production Performance

Fatma Bahar Hosgor, Omer Inanc Tureyen, Abdurrahman Satman and Murat Cinar

Istanbul Technical University, ITU Petrol ve Dogal Gaz Muh. Bol., Maslak, Istanbul, Turkey

oztorun@itu.edu.tr, inanct@itu.edu.tr, mdsatman@itu.edu.tr and cinarmura@itu.edu.tr

Keywords: Carbon dioxide, production performance

ABSTRACT

Geothermal reservoirs often contain carbon dioxide which has considerable role on the reservoir performance and energy production. Even small amounts of carbon dioxide have profound effects on the behavior of reservoir pressure. Carbon dioxide has the tendency to shift the flashing point of the reservoir fluid to a considerably higher value and causes a gas phase to form in the reservoir. Due to the gas phase formed during production, reservoir pressure can be maintained better. When modeling such reservoirs, it is crucial to include the effects of carbon dioxide in the model. In this study, a new non-isothermal lumped parameter (tank) model is developed to examine and predict the behavior of mass and heat production of geothermal fluids with the consideration of the effects of carbon dioxide. Components of the geothermal system such as the reservoir, the aquifer and the heating source are represented by using a tank (or tanks) so the pressure and temperature behavior of any component of the geothermal system can be modelled. This way the behavior of multiple reservoirs (for example shallow and deep reservoirs with different properties such as different carbon dioxide concentrations) can be modelled. The model is based on three conservation equations; mass balances on water and carbon dioxide and an overall energy balance (which is an energy balance that includes contributions only to the heat content of the system). With this model, the change of pressure and temperature that occurs from production, reinjection and natural recharge, the change of carbon dioxide concentration both in the liquid and gas phases with production and also the variation of gas saturation in the geothermal reservoir can be examined. On various synthetic examples we study the effects of various parameters on the performance of pressure and temperature of geothermal systems. We especially look at cases where the mass fraction of carbon dioxide can change with time and its effects on the performance.

1. INTRODUCTION

The utilization of geothermal energy has increased greatly due to its cleanliness, safeness, renewability and sustainability. In early geothermal reservoir simulations the reservoir fluids were idealized as pure water but many geothermal reservoirs contain significant amounts of noncondensible gases including H_2S, N_2, NH_3, H_2, CH_4 and CO_2 where the concentration of gases could be as high as 10 percent by mass. Subsequent more realistic representations of geothermal fluids must include carbon dioxide, which usually is the most prominent noncondensible gas. For liquid dominated geothermal reservoirs, mass fractions of CO_2 dissolved in liquid water can be as much as 5%. The Kizildere field in Turkey, for example, contains around 1.5% CO_2 dissolved in the liquid water and this value increases up to 3% in the deep zones (Satman et al., 2005).

When modeling geothermal reservoirs (either using numerical models or lumped parameter models) it is crucial to account for the effects of CO_2. When production starts in a geothermal field, CO_2 dominates the thermodynamic properties of the fluid. Particularly the pressure – temperature behavior of the water CO_2 mixture changes significantly with changing mass fraction of CO_2 in the mixture. Geothermal systems with CO_2 content have a higher bubble point (flashing) pressure than systems with pure water. Increasing amounts of CO_2 increase the bubble point pressure.

The effects of CO_2 in modeling geothermal systems have been considered by many authors in the literature. Zyvolosky and O'Sullivan (1980) numerically modeled the transport of CO_2 in a two-phase geothermal system. They gave a very detailed description of the conservation equations to be used in numerical simulation of geothermal reservoirs. The authors used three conservation equations; a mass balance equation for water, an overall energy balance equation and a mass balance equation for CO_2. In this study the primary variables are taken to be pressure, enthalpy and temperature. Their model showed that CO_2 has significant effect on pressure transients.

Atkinson et al. (1980) presents a lumped parameter model for vapor dominated reservoirs to be used in modeling the Bagnore geothermal reservoir which contains considerable amounts of CO_2. However it is important to note that the initial conditions of the Bagnore field are reported to be two phase. Hence the authors have adopted a model that is composed of two tanks; one for modeling the liquid region and the other for modeling the vapor region and mass transfer is allowed between the two tanks.

O'Sullivan et al. (1985) have given a detailed description of how primary variables should be adjusted updated during the numerical simulation of a geothermal reservoir based on if the fluid is under a compressed liquid state, two phase state or single phase gas state. The approach given by the authors is still used in many of the numerical models today.

Alkan and Satman (1990), have improved on the lumped parameter model of Whiting and Ramey (1969), originally developed for pure water systems, by introducing a thermodynamic package that describes the behavior of water-CO2 systems. Their model was simple and very general and could be used for a pressurized water-CO2 system and for a liquid-dominated system. This model was applied on field data from the Cerro Prieto, Ohaaki, Bagnore and Kizildere fields.

2. WATER-CO_2 SYSTEMS

In this section we briefly describe the behavior of water-CO_2 systems. In the following subsection review of the equations that represent the thermodynamic package of water-CO_2 systems used in this study is given. Then this is followed by an illustration of the most profound effect of CO_2 on water-CO_2 mixtures.

2.1 The thermodynamic package

The thermodynamic package includes the correlations and relationships used to evaluate the thermophysical properties of phases in which water and CO_2 are partitioned. The partial pressure of CO_2 is linked with the mass fraction of CO_2 in the liquid water through Henry's law given in Eq. 1.

$$y_{CL} = \frac{P_{CO_2}}{H(T)} \tag{1}$$

Here P_{CO2} is the partial pressure of CO_2 (Pa) y_{CL} is the mole fraction of CO_2 in liquid water, $H(T)$ is Henrys constant (Pa^{-1}) and T is temperature (K). As shown in Eq. 1, Henry's constant is given as a function of temperature. Henry's constant for the dissolution of carbon dioxide in pure water is calculated using polynomial regression of data from 0 to 300°C published by Cramer (1982).

$$H(T) = \sum_{i=0}^{5} B(i) T^i \tag{2}$$

where the coefficients B(i) have the following values:

Table 1: Coefficients for Eq. 2.

B(0)	7.83666×10^{7}
B(1)	1.96025×10^{6}
B(2)	8.20574×10^{4}
B(3)	-7.40674×10^{2}
B(4)	2.18380
B(5)	-2.20999×10^{-3}

Another correlation which is given by Upton and Santoyo (2002) is given as an option for providing the link between the carbon dioxide content and the partial pressure of carbon dioxide.

$$\ln K_H = a + b(T + 273.15) + c(T + 273.15)^2 + d(T + 273.15)^3 \tag{3}$$

where the constants a, b and c are provided in Table 2.

Table 2: Regression coefficients for Eq. 3.

a	4.517428673
b	2.5554535×10^{-2}
c	-1.02213×10^{-4}
d	9.30689×10^{-8}

Then the relation between the K_H constant given in Eq. 3 and the partial pressure of CO_2 is given in Eq. 4.

$$p_{CO_2} = \frac{18}{44} K_H f_{CL} \tag{4}$$

Where K_H is the Henry's constant and f_{CL} is the mass fraction of CO_2 in water. For simplicity the liquid phase density and the liquid phase viscosity of a water-CO_2 mixture will be taken equal to that of the density and viscosity of liquid water. For the enthalpy of a liquid phase of a water-CO_2 system we use the relationship given by O'Sullivan et. al. (1990) shown in Eq. 5.

$$h_L = h_w(1 - f_{CL}) + (h_{CO_2} + h_{sol}) f_{CL} \tag{5}$$

Here h_L is the enthalpy of the liquid phase (J/kg), h_w is the enthalpy of liquid water (J/kg), h_{CO2} is the enthalpy of the gaseous CO_2 (J/kg) and h_{sol} is the enthalpy of solution. h_{CO2} is calculated based on Eq. 6 given by Sutton (1976):

$$h_{CO_2} = -2.18 \times 10^5 + 732\,T + 0.252\,T^2 - 2.63 \times 10^{-5} T^3 \tag{6}$$

The solution enthalpy can be determined using Eq. 7 given by Ellis and Golding (1963).

$$h_{sol} = \left[-1.351 + 0.01692\,(T - 273.15) - 7.5524 \times 10^{-5}(T - 273.15)^2 + 1.318 \times 10^{-7}(T - 273.15)^3\right] \times 10^6 \tag{7}$$

The pressure of the gas phase can be computed by simply adding the partial pressure of steam and the partial pressure of CO_2 as shown in Eq. 8.

$$p = p_s + p_{CO_2} \tag{8}$$

Here p is the pressure of the gas (Pa) and p_s is the partial pressure of steam (Pa). p_s, in this study is determined from IAPWS (2007). The gas phase density in the system can be computed using Eq. 9.

$$\rho_G = \rho_s + \rho_{CO_2} \tag{9}$$

where ρ_G is the gas phase density (kg/m^3), ρ_s is the steam density (kg/m^3) and ρ_{CO_2} is the density of gaseous CO_2. The gas phase viscosity is taken as the viscosity of the steam and calculated as given in Eq.10.

$$\mu_G = (90 + 0.35(T - 273.15))10^{-7} \tag{10}$$

where μ_G is the viscosity of the gas phase (Pa.s), and T is the temperature (K). The enthalpy of the gas phase can be determined using Eq. 11.

$$h_G = h_s(1 - f_{CG}) + h_{CO_2} f_{CG} \tag{11}$$

where h_G is the enthalpy of the gas phase (J/kg), h_s is the enthalpy of steam (J/kg), f_{CG} is the mass fraction of CO_2 in the gas phase and h_{CO_2} is the enthalpy of gaseous CO_2. Finally at a given pressure and temperature, the mass fraction of CO_2 in the gas phase can be determined using Eq. 10.

$$f_{CG} = \frac{\rho_{CO_2}}{\rho_G} \tag{12}$$

Eq's 6 to 12 have been taken from O'Sullivan et. al. (1985).

2.2 The effect of CO_2 on water properties

In this subsection we mainly illustrate the effect of dissolved CO_2 on the phase behavior of water. This illustration is performed through a pressure temperature diagram for various mass fractions of dissolved CO_2. The bubble point pressures of the water-CO_2 mixture are obtained using Eq. 8 for various temperatures. The partial pressure of CO_2 is obtained using Eq. 1. Figure 1 illustrates the results.

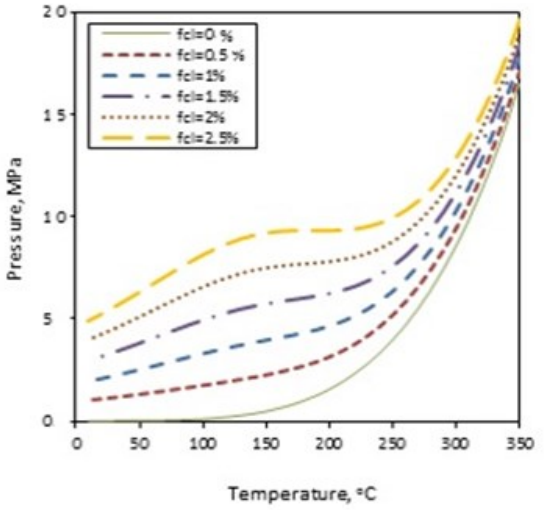

Figure 1: Pressure–temperature behavior of water–CO_2 mixtures for various mass fractions of CO_2.

As mentioned earlier, the most profound effect of CO_2 on the behavior of water – CO_2 mixtures is the shift it causes on the bubble point pressures. For example, at around 200°C pure water has a bubble point pressure at around 1.5 MPa. If dissolved CO_2 exists in the water phase with a mass fraction of 0.5% then the mixture would have a bubble point pressure at around 3.1 MPa. At a 2.5% mass fraction, the mixture has a bubble point pressure at around 8.9 MPa. Small amounts of CO_2 dissolved in water considerably change the bubble point pressure of water. If not accounted for, during production, flashing point depths within wells could be associated with high errors where shallower flashing point depths would be anticipated when actual flashing point depths would be located much deeper. During depletion, if the flashing point is to move into the reservoir, then a gas phase would start to form. This would have the effect such that, the decline rate in pressures due to production would be decreased significantly. This is due to the

fact that below the bubble point pressure a gas phase starts to evolve. Since gas has much higher compressibility when compared with liquids they can compensate for production simply by expanding more than liquids hence causing a decrease in the pressure decline rate.

Figure 2 shows the pressure-temperature-enthalpy behavior of the water–CO_2 mixtures having 0.015 mass fraction of CO_2 dissolved in the liquid phase. The shift caused by the existence of carbon dioxide on the bubble point pressure of the mixture is also visible in the pressure – enthalpy diagram. As the pressure is decreased, once the bubble point pressure is reached then gas starts to form and pressure starts to follow the iso-thermal lines in the two phase region. It is important to note that the gas is initially composed of carbon dioxide. During this time where carbon dioxide dominates the gas phase, the pressure declines rapidly. As pressure is further decreased due to production, steam content starts dominating the gas phase and pressure starts becoming constant (Satman and Alkan 1980). After this point the behavior of the fluids are more or less like that of pure water.

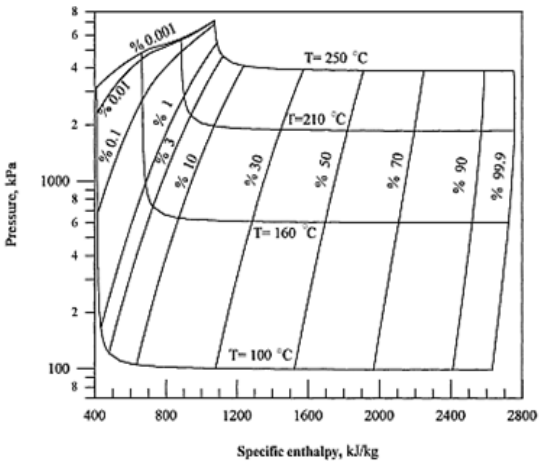

Figure 2: Pressure–temperature–enthalpy behavior of water–CO_2 mixtures (for fCL=0.015).

3. DESCRIPTION OF THE MODEL

The basic equations represent the mass, momentum and energy balance for the geothermal system containing some amount of CO_2. This set of equations is completed by using an appropriate thermodynamic package. In the energy balance equation, it is assumed that the rock and fluids are in thermal equilibrium. In other words, when the energy balance is applied heat transfer between the rock, the liquid and the gas is ignored (Nayfeh et. al, 1975). The model is based on three conservation equations; mass balances on water and carbon dioxide and an overall energy balance. In the model presented here, each component of a geothermal system is represented using a tank that is composed of fluid and rock. The tanks represent either the reservoir, the aquifer, the heating source or the atmospheric block to which natural discharge occurs. In some cases more than one tank can be used to represent the reservoir or the aquifer. Here we will consider that any tank can make an arbitrary number of connections with any other tank. This generalized approach had previously been taken by Tureyen and Akyapi (2011) and Hosgor et al. (2013). Figure 3 illustrates any tank *i* and the connections it makes to neighboring tanks.

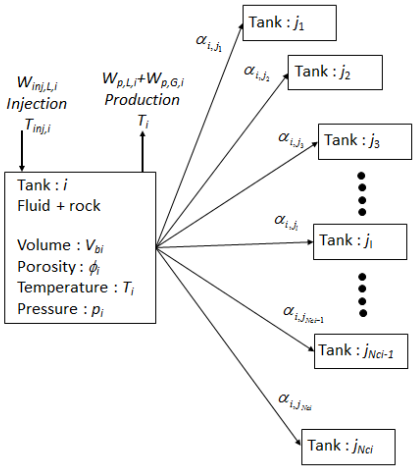

Figure 3: Properties of a representative tank in the model.

The overall model will be assumed to be composed of a total of N_t number of tanks. Tank *i* in the system is assumed to make an N_{ci} number of connections to other tanks. Note that N_{ci} can vary from tank to tank because each tank in the model can make a different

number of connections. Liquid water may be injected into the tank at a specified temperature T_{inj}. Production is specified at a total production rate which is the sum of gas and liquid rates. The individual amounts are determined based on their mobility. The fluid is produced at the tank temperature T_i. The liquid mass flow rate between any tank j_l and tank i is determined using an approach similar to that of Schilthuis (1936) and is given in Eq. 13.

$$W_{L,i,j_l} = \alpha_{L,i,j_l}\left(p_{j_l} - p_i\right) \tag{13}$$

Here W_{L,i,j_l} is the mass flow rate of the liquid phase transferred between tank i and tank j_l (kg/s), P_{jl} is the pressure of tank j_l (Pa), P_i is the pressure of tank i (Pa) and α_{L,i,j_l} is the recharge index (kg/(bar.s)) which represents the mass flow rate for a given unit pressure drop between the tanks. At this point it is important to note that the recharge index is composed of two parts; a rock part (which assumed to independent of pressure and temperature) and a fluid part (which is assumed to be a strong function of pressure and temperature. Hence the recharge index can be written as follows:

$$\alpha_{L,i,j_l} = \psi_{i,j_l}\lambda_L \tag{14}$$

where ψ_{i,j_l} is the rock part of the recharge index (m^3) and λ_L is the fluid part of the recharge index (kg/(Pa.s.m3)). The fluid part is given in Eq. 15.

$$\lambda_L = \frac{k_{r,L}\rho_L}{\mu_L} \tag{15}$$

where $k_{r,L}$ is the relative permeability of the liquid. The rock part of the recharge index is given in Eq. 16.

$$\psi_{i,j_l} \propto \frac{kA}{d} \tag{16}$$

Here k represents the permeability of the medium (m^2), A is the cross-sectional area that the fluid passes through when being transferred between the tanks (m^2) and d is some characteristic length which is a measure of the distance the fluid takes when it is being transferred from one tank to the other (m). It is important to note that the individual values of *k, A* and *d* need not be known. They are all lumped in ψ_{i,j_l} which is treated as an input parameter or can be treated as a parameter to be adjusted during history matching. The fluid part of the recharge index on the other hand is computed for a given pressure, temperature and saturation. The gas mass flow rate is determined in the same fashion using Eq. 13, except with the subscript *L* replaced with *G*.

The mass balance for tank i can be written as shown in Eq. 17.

$$V_i\frac{d}{dt}(\rho_L S_L\phi + \rho_G S_G\phi)_i - \sum_{l=1}^{N_{ai}}\alpha_{L,i,j_l}\left(p_{j_l} - p_i\right) - \sum_{l=1}^{N_{ai}}\alpha_{G,i,j_l}\left(p_{j_l} - p_i\right) + W_{p,L,i} + W_{p,G,i} + W_{inj,L,i} = 0 \tag{17}$$

Where S represents saturation (fraction), and ϕ represents the porosity (fraction). The first term is the accumulation of mass in the tank, the second term represents the liquid mass contribution from other tanks and the third term represents the gas mass contribution from other tanks. The fourth, fifth and sixth terms are the production rate of the liquid, the production rate of the gas and the injection rate of the liquid respectively. The energy flux due to conduction between any tank jl and tank i is given by Eq. 18.

$$Q = \gamma_{i,j_l}\left(T_{j_l} - T_i\right) \tag{18}$$

where Q is the energy rate (J/s) and γ_{i,j_l} is the conduction index (J/(K.s)). The energy balance can be given as:

$$\begin{aligned}&\frac{d}{dt}\left[(1-\phi)V\rho_m C_m T + V\phi\left(\rho_L u_L S_L + \rho_G u_G S_G\right)\right] + W_{p,L,i}h_{L,i} + W_{p,G,i}h_{G,i} + W_{inj,L,i}h_{L,inj,i}\\ &- \sum_{l=1}^{N_{ai}}\alpha_{L,i,j_l}\left(p_{j_l} - p_i\right)h_{L,\xi} - \sum_{l=1}^{N_{ai}}\alpha_{G,i,j_l}\left(p_{j_l} - p_i\right)h_{G,\xi} - \sum_{l=1}^{N_{ai}}\gamma_{i,j_l}\left(T_{j_l} - T_i\right) = 0\end{aligned} \tag{19}$$

where ρ_m represents the rock matrix density (kg/m^3), C_m represents the specific heat capacity of the rock (J/(kg.K)), u represents the internal energy (J/kg) and h represents the enthalpy (J/kg). The first term is the accumulation of energy in the tank, the second and the third term represent the contribution of energy due to liquid and gas production, the fourth term represents the contribution of energy due to liquid injection, the fifth and the sixth terms represent the contribution of energy from other tanks by movement of liquid and vapor, and the seventh term represents the overall energy contribution from heat transfer by conduction, respectively. When considering the energy contribution from other tanks, we perform an upwinding scheme on the enthalpy as given in Eq. 20.

$$h_\xi = \begin{cases} h_i & \text{if} \quad p_i > p_{j_l} \\ h_{j_l} & \text{if} \quad p_i < p_{j_l} \end{cases} \tag{20}$$

Finally the mass balance on the CO_2 component is given in Eq. 21.

$$V_i \frac{d}{dt}(\rho_L S_L \phi f_{CL} + \rho_G S_G \phi f_{CG})_i - \sum_{l=1}^{N_a} \alpha_{L,i,j_l}(p_{j_l} - p_i) f_{CL,\xi} - \sum_{l=1}^{N_a} \alpha_{G,i,j_l}(p_{j_l} - p_i) f_{CG,\xi} + W_{p,L,i} f_{CL,i} + W_{p,G,i} f_{CG,i} = 0 \quad (21)$$

where *f* represents the mass fraction of CO_2 either in the liquid or the gas phase. Here, the first term is the accumulation of carbon dioxide in the tank, the second and the third term represent the contribution of mass from other tanks by movement of liquid CO_2 and vapor CO_2, the fourth and the fifth term represent the contribution of mass due to liquid CO_2 and gas CO_2 production, respectively. We perform an upwinding approach similar to that given in Eq. 20. The approach is given in Eq. 22.

$$f_\xi = \begin{cases} f_i & \text{if} \quad p_i > p_{j_l} \\ f_{j_l} & \text{if} \quad p_i < p_{j_l} \end{cases} \quad (22)$$

Eq's. 17, 19 and 21 are non-linear equations and are solved in a fully implicit manner using the Newton-Raphson technique. For the selection of primary variables O'Sullivan et. al. (1985) proposed an approach that can be summarized as; if the tank contains a single phase fluid, then the primary variables are chosen as pressure, temperature and partial pressure of CO_2, whereas if the tank contains gas and liquid phases at the same time, the gas saturation is used as a primary variable instead of temperature. After some verification studies we decide to use pressure, temperature and partial pressure of CO_2 in the single phase region but for the two phase region we use saturation of gas, temperature and partial pressures of CO_2 as primary variables. By choosing these primary variables we overcome the fluctuations during phase transition.

4. VERIFICATION STUDIES WITH PETRASIM

The verification of the tank model is carried out with the commercial simulator Petrasim which uses the codes of TOUGH family generated mainly by Pruess et al. (1999). It can develop models for non-isothermal flow of multicomponent and multiphase fluids in porous media. Figures 4-8 illustrate the results of pressure, temperature, gas saturation, mass fraction of CO_2 in water and mass fraction of CO_2 in gas phase. As can be seen from the figures the results of the tank model are compatible with the simulator Petrasim.

Table 3: Data used in Petrasim and the tank model.

Bulk volume, m^3	1×10^9
Porosity, fraction	0.2
Initial pressure, MPa	5
Initial temperature, K	450
Rock compressibility, Pa^{-1}	5×10^{-10}
Rock thermal expansion coefficient, K^{-1}	0
Density of rock, kg/m^3	2600
Heat capacity of rock, J/(kg.K)	1000
Permeability, m^2	1×10^{-13}
Flow rate, kg/s	2
Partial pressure of CO_2, MPa	2.67
Reinjection rate, kg/s	1.6
Reinjection entalpy, J/kg	2.475×10^5

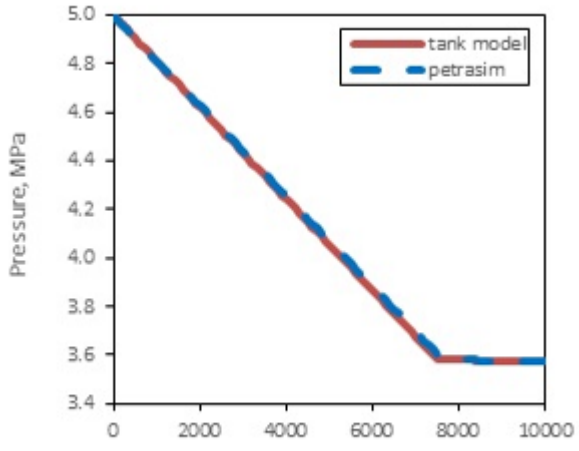

Figure 4: Comparison of pressure behavior

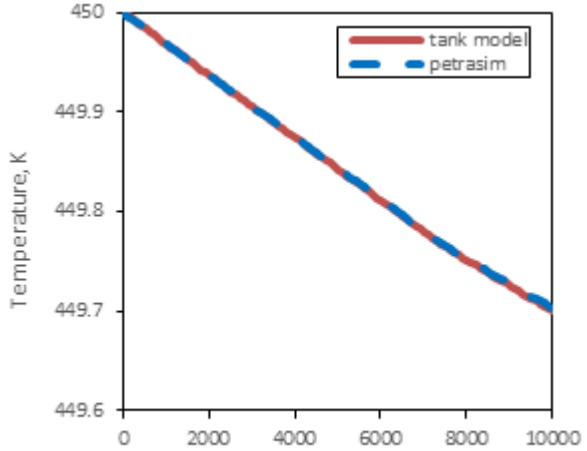

Figure 5: Comparison of temperature behavior

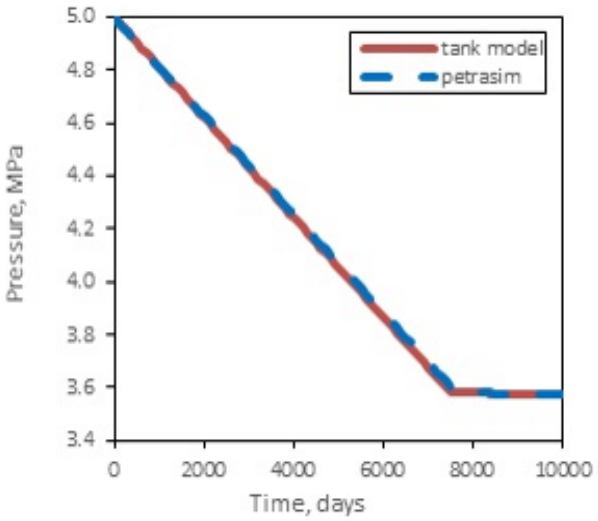

Figure 6: Comparison of gas saturation behavior

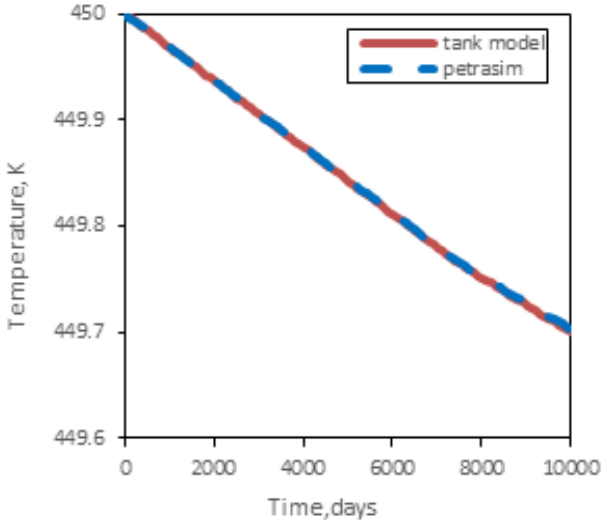

Figure 7: Comparison of mass fraction of CO2 in gas phase.

4. APPLICATIONS

In this section we provide three different cases to illustrate the effects of CO_2 on the performance of geothermal reservoirs. For simplicity a single tank model is chosen. The main properties of the reservoir that are used in the models are given in Table 3, other circumstances are explained for each case.

Table 4: Reservoir properties.

Bulk volume, m^3	1×10^9
Porosity, fraction	0.2
Initial pressure, Pa	50×10^5
Initial Temperature, K	450
Rock compressibility, Pa^{-1}	5×10^{-10}
Rock thermal expansion coefficient, K^{-1}	0
Density of rock, kg/m^3	2600
Heat capacity of rock, J/(kg.K)	1000

4.1 The effect of mass fraction of CO_2

In this case, the effect of mass fractions of CO_2 on the behavior of the reservoir is examined for four different mass fractions of CO_2 (0%, 0.5%, 1% and 1.5). Constant production at 2 kg/s is assumed for duration of 10000 days.

The pressure behavior of such a system is given in Figure 8. If no CO_2 were present in the water, then production is maintained in a compressed liquid state until 5000 days. After 5000 days, steam and water co-exist in the reservoir. However, it is important to note that once the reservoir fluid becomes two-phase, the decline rate of pressure is decreased. This is due to the much higher compressibility (when compared with liquid compressibility) of the gas phase that co-exists with the liquid (Satman and Ugur, 2002). When 0.5% CO_2 is dissolved in water, then two-phase conditions are reached earlier (at around 2500 days). The pressure for the remaining 7500 days remains fairly constant maintained by gas compressibility. As expected, even further increasing the CO_2 content results in pressure maintenance at even earlier times. Figure 9 illustrates how the gas saturation changes with time for the same amounts of dissolved CO_2. As expected, the gas saturation starts increasing as soon as the bubble point pressures are reached in the reservoir. The increases associated with the saturations are linear. At this point it is important to note that, the computed pressures and saturations of the model reflect the average pressure and saturations of the reservoir. During production, gas saturations would be varying with position and would be at a maximum around the well in a case where the bottomhole pressures of wells have dropped below the bubble point pressure.

Figure 10 gives the evolution of the mass fraction of the CO_2 dissolved in the water. For each initial mass fraction, the mass fractions of dissolved CO_2 tend to decrease. However as expected this decrease is very small. This decrease is associated with the transfer of carbon dioxide into the gas phase. Finally, Figure 11 gives the evolution of the mass fraction of CO_2 in the gas phase. At first the mass fractions are zero since no gas phase is present. Then when the bubble point pressure is reached and gas phase starts to form, we observe that the gas phase is made up of mostly CO_2. For a mass fraction of 1.5% CO_2 dissolved in water, the gas phase is composed 90% of CO_2 whereas for a mass fraction of 0.5% CO_2 dissolved in water, the gas phase is composed 78% of CO_2.

4.2 The effect of production rate

In this case, the effect of production rate on the behavior of the reservoir is examined for four different flow rates (2 kg/s, 5 kg/s, 10 kg/s and 20 kg/s) for duration of 10000 days. Initial mass fraction of CO_2 is taken as 1%.

The pressure behavior of the system is given in Figure 12. As it is seen from the figure, as the flow rate increases pressure decreases rapidly in the liquid phase region and two-phase forms. After the fluid becomes two phase the pressure decline decreases and the

pressure decline becomes proportional with the flow rate. In Figure 13, the gas saturation behavior of the system is given. When the flow rate increases the gas phase is formed earlier. The gas saturation starts increasing as soon as the bubble point pressures are reached in the reservoir. The higher gas saturation is reached with the higher production.

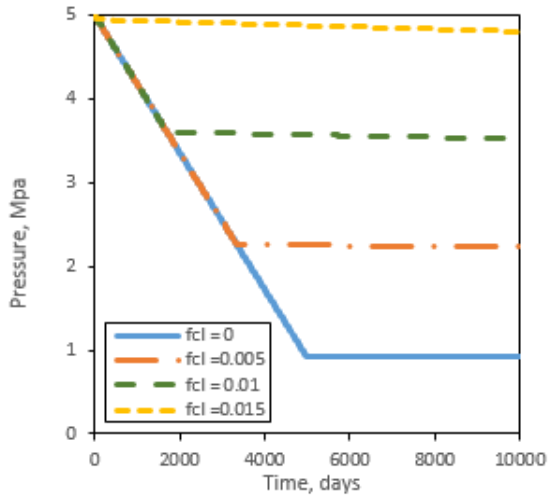

Figure 8: Pressure behavior for various amounts of CO_2 dissolved in water.

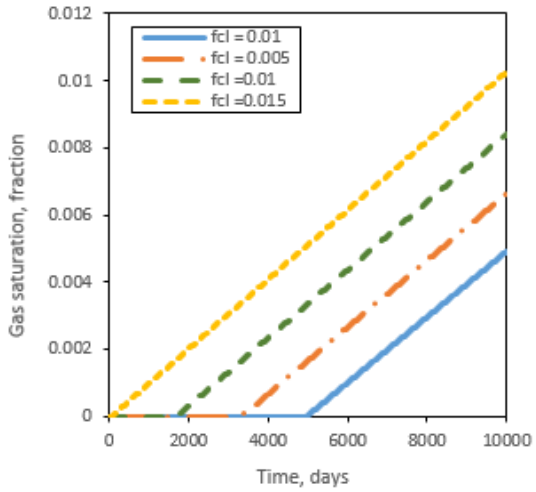

Figure 9: Gas saturation behavior for various amounts of CO_2 dissolved in water.

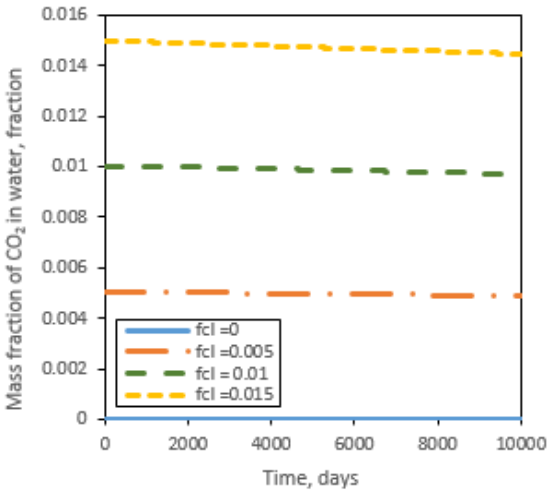

Figure 10: Evolution of the mass fraction of CO_2 in water.

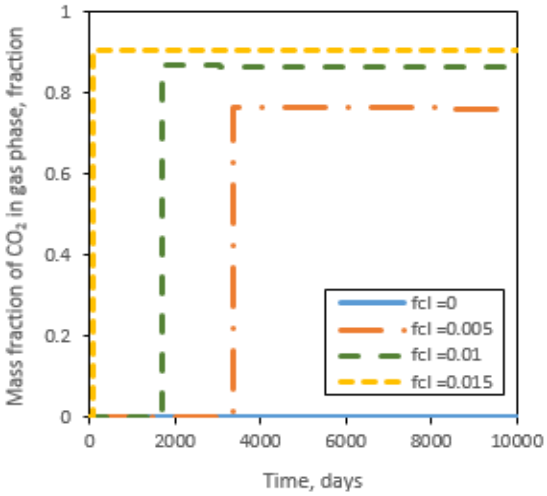

Figure 11: Evolution of the mass fraction of CO_2 in the gas phase.

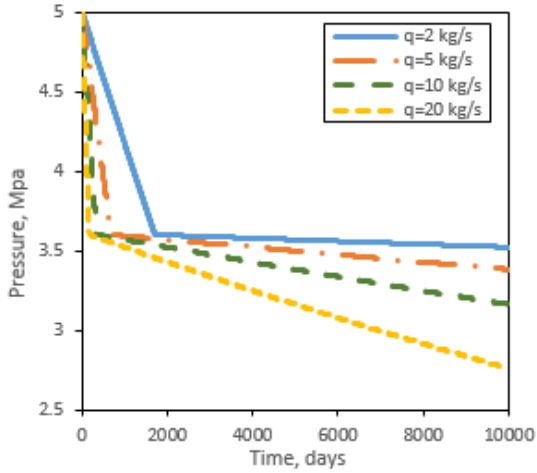

Figure 12: Pressure behavior for various flow rates.

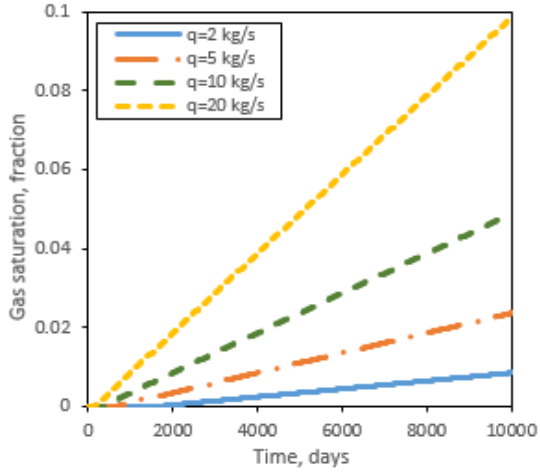

Figure 13: Gas saturation behavior for various flow rates.

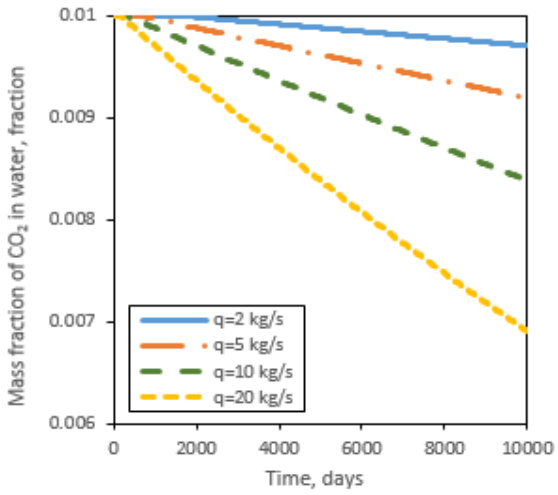

Figure 14: Evolution of the mass fraction of CO2 in water.

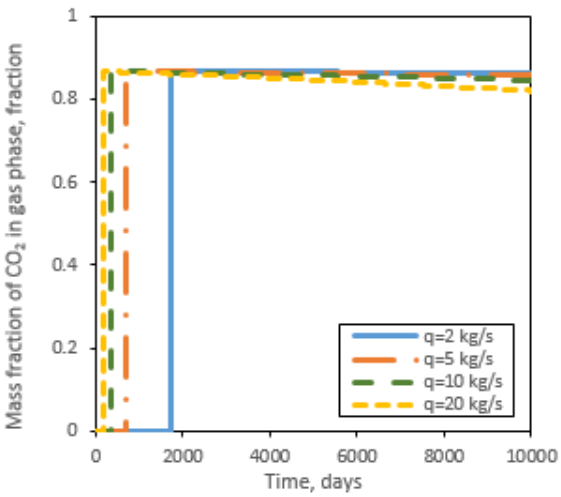

Figure 15: Evolution of the mass fraction of CO2 in the gas phase.

Figure 14 gives the evolution of the mass fraction of the CO_2 dissolved in the water for various flow rates. In the compressed liquid region there is no change in the mass fraction of CO_2 as it is still dissolved in the water, after the bubble point is reached the mass fraction starts to decrease and as expected the mass fractions of dissolved CO_2 tend to decrease more as the flow rate is increased. Figure 15 gives the evolution of the mass fraction of CO_2 in the gas phase for various flow rates. At the beginning the mass fractions are zero since no gas phase is present. With the increase in the flow rate the bubble point pressure is reached earlier and gas phase that is made up of mostly CO_2 starts to form. Transition of liquid CO_2 to gaseous CO_2 occurs very quickly and tends to stabilize. At late times, the decrease of mass fraction of CO_2 in gas phase with the production is observed clearly at higher flow rates.

4.3 The effect of reinjection

In this case, the effect of reinjection on the performance of the geothermal system is examined. No reinjection, 50% reinjection, 80% reinjection and 100% reinjection scenarios are studied. Constant production at 10 kg/s is assumed for duration of 10000 days and the initial mass fraction of CO_2 is taken as 1%.

In Figure 16, the pressure behavior of the system is given. If there is no reinjection a rapid pressure drop occurs and after around 250 days gas phase forms. After the reservoir fluid becomes two-phase, the decline rate of pressure is decreased. With the reinjection the pressure decline is diminished and thus the production of gas is begun at later times. For example, for 50 % reinjection scenario bubble point pressure is reached around 500 days which is twice of the without reinjection scenario. For the 100 % reinjection, since production is maintained in a compressed liquid state for 10000 days of production, no gas is formed. Figure 17 illustrates the temperature behavior of the system with initial temperature of 450 K with and without reinjection case. If no reinjection is applied, a faster decrease in temperature occurs in compressed liquid region and after the bubble point is reached a less temperature decrease occurs. The temperature of the system decreases more with the increase in the amount of reinjection of water with a temperature of 333.15 K.

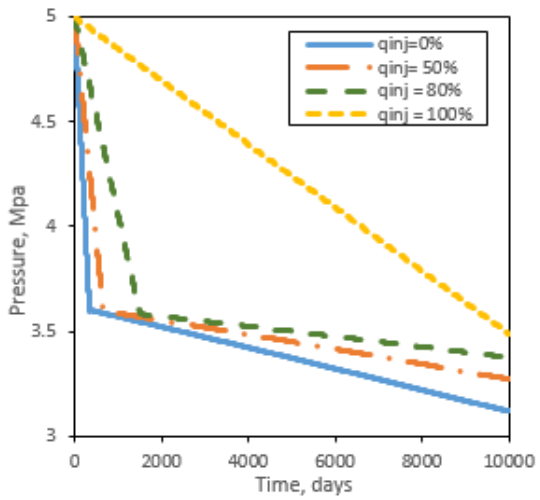

Figure 16: Pressure behavior for various percentage of reinjection.

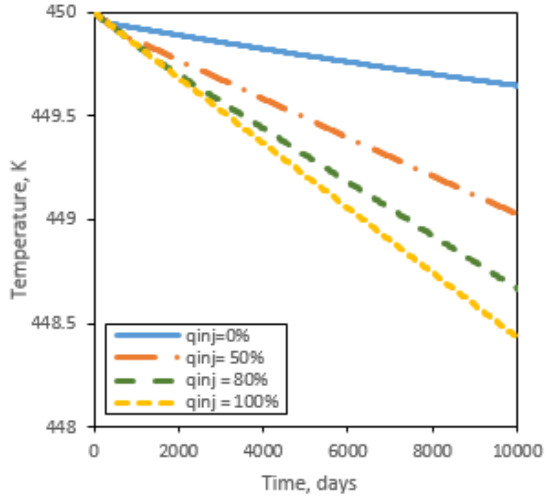

Figure 17: Temperature behavior for various percentage of reinjection.

In Figure 18, gas saturation behavior of the system is given. After the bubble point pressure is reached the gas phase begins to form. The time of the occurrence of the first bubble is extended with the increase in the amount of reinjection. If there is no reinjection, gas saturation increases with the decrease in the total pressure of the system. When the pressure decline is decreased with reinjection, gas saturation decreases. For the 100 % reinjection scenario because the system is maintained in compressed liquid phase, no gas saturation is occurred. Figure 19 illustrates the change of mass fraction of CO_2 in gas phase. The mass fractions of CO_2 in gas phase are zero at early time since no gas phase is present. With the pressure decline with production, the bubble point pressure is reached and gas phase that is made up of mostly CO_2 starts to form. With the reinjection this occurrence is reached subsequently. At late times, the decrease of mass fraction of CO_2 in gas phase with the production is observed in no reinjection scenario, this trend is less in reinjection cases.

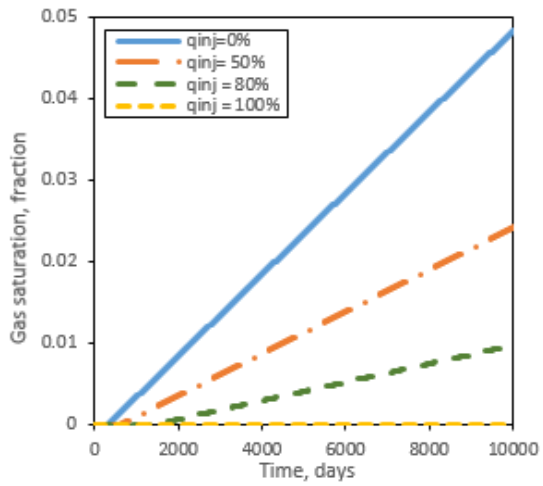

Figure 18: Gas saturation behavior for various percentage of reinjection.

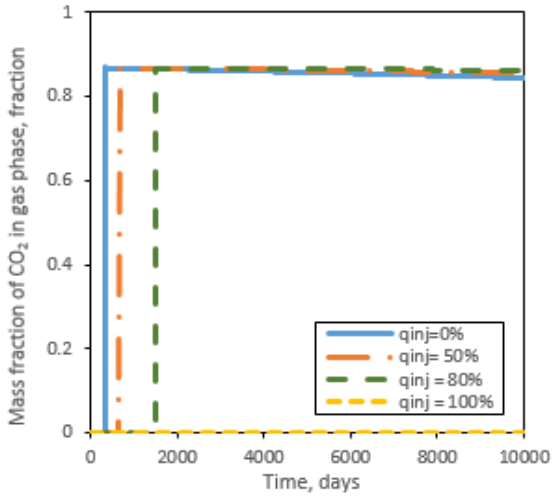

Figure 19: Evolution of the mass fraction of CO2 in the gas phase for various percentage of reinjection.

5. CONCLUSIONS AND FUTURE WORK

The following conclusions have been obtained and necessary future work is listed:

• A lumped parameter model capable of modeling the pressure and temperature behavior of geothermal systems that contain CO_2 has been developed.

• The effects of CO_2 are most profound on the bubble point pressure. A small amount of CO_2 dissolved in the liquid water phase can significantly increase the bubble point pressure for any given temperature.

• Due to the increase in bubble point pressure, two phases can form in the reservoir at relatively higher pressures.

• Due to the gas phase that forms in the reservoir, the pressure decline rate is slowed down. This is because of the much higher compressibility of the gas phase.

• The model has not yet been validated by methods present in the literature. Hence, the next step in the study is the validation of the model.

• The model will be used for modeling the pressure and temperature behavior of the Kizildere Geothermal field.

ACKNOWLEDGEMENTS

We would like to thank the Scientific and Technological Research Council of Turkey (TUBİTAK Project No: 113M425) for supporting this study.

REFERENCES

Alkan, H. and Satman, A.: A New Lumped Parameter Model For Geothermal Reservoirs in The Presence of Carbon Dioxide, Geothermics, **19**, (1990), 469-479.

Atkinson, P. G., Celati, R., Corsi, R. and Kucuk, F.: Behavior of the Bagnore Steam/CO_2 Geothermal Reservoir, Italy, Society of Petroleum Engineers Journal, **20**, (1980), 228-238.

Cramer, S.D.: The Solubility Of Methane, Carbon Dioxide and Oxygen in Brines From 0° To 300°C, US Bureau of Mines, Report No. 8706, U.S.A., 16 pp. (1982).

Ellis, E. J. and Golding, R. M.: The Solubility Of CO_2 Above 100°C in Pure Water and in Sodium Chloride Solutions, American Journal of Science, **261**, (1963), 47-60.

Hosgor, F. B., Çınar, M., Haklıdır, F., Tureyen, O.I., Satman, A.: A New Lumped Parameter (Tank) Model For Reservoirs Containing Carbon Dioxide, *Proceedings*, 38rd Workshop on Geothermal Reservoir Engineering, Stanford University, USA (2013).

IAPWS: Revised Release on the IAPWS Industrial Formulation 1997 for the Thermodynamic Properties of Water and Steam, (2007).

Nayfeh, A.H., Brownell, D.H., Garg, S.K.: Heat Exchange in Fluid Percolating Through Porous Media, *Proceedings*, Society of Engineering Science Meeting, Austin, Texas, Oct.20-22, (1975).

O'Sullivan, M. J., Bodvarsson, G. S., Pruess, K. and Blakeley, M. R.: Fluid and Heat Flow in Gas-Rich Geothermal Reservoirs, Society of Petroleum Engineers Journal, **25**, (1985), 215-226.

Pruess, K., Oldenburg, C., and Moridis, G.: TOUGH2 User's Guide, Version 2.0, Earth Sciences Division, Lawrence Berkeley National Laboratory, LBNL-43134, November, (1999).

Satman, A., Sarak, H., Onur, M.and Korkmaz, E.P.: Modeling of Production/Reinjection Behavior of the Kizildere Geothermal Field by a 2-Layer Geothermal Reservoir Lumped Parameter Model, *Proceedings*, World Geothermal Congress, Antalya, Turkey, 24-29 April, (2005).

Satman, A. and Ugur, Z.: Flashing Point Compressibility of Geothermal Fluids with Low CO_2 Content and Its Use in Estimating Reservoir Volume, Geothermics, **31**, 29-44, (2002).

Sutton, F. M.: Pressure-Temperature Curves for a Two-Phase Mixture of Water and Carbon Dioxide, New Zealand Journal of Science, **19**, (1976), 297-301.

Schilthuis, R. J.: Active Oil and Energy, Trans. AIME, **118**, (1936), 33-52.

Tureyen, O. I. and Akyapi, E.: A Generalized Non-Isothermal Tank Model for Liquid Dominated Geothermal Reservoirs, Geothermics, **40**, (2011), 50-57.

Upton, P. S. and Santoyo, E.: A Comprehensive Evaluation of Empirical Correlations for Computing the Solubility of CO_2 in Water, *Proceedings*, 24th NZ Geothermal Workshop, NewZealand, (2002).

Whiting, R. L. and Ramey, H. J.: Application of Material and Energy Balances to Geothermal Steam Production, Journal of Petroleum Technology, **21**, (1969), 893-900.

Zyvolosky, G. A. and O'Sullivan, M. J.: Simulation of a Gas-Dominated, Two-Phase Geothermal Reservoir, Society of Petroleum Engineers Journal, **20**, (1980), 52-58.